



Total Catalytic Oxidation of Ethanol over MnCoAl Mixed Oxides Derived from Layered Double Hydroxides: Effect of the Metal Ratio and the Synthesis Atmosphere Conditions

Mariebelle Tannous, Charf Eddine Bounoukta, Stéphane Siffert, Christophe Poupin, Renaud Cousin

► To cite this version:

Mariebelle Tannous, Charf Eddine Bounoukta, Stéphane Siffert, Christophe Poupin, Renaud Cousin. Total Catalytic Oxidation of Ethanol over MnCoAl Mixed Oxides Derived from Layered Double Hydroxides: Effect of the Metal Ratio and the Synthesis Atmosphere Conditions. *Catalysts*, 13 (9), pp.1316, 2023, Layered Double Hydroxide-Based Catalysts for Advanced Chemical Technologies, 10.3390/catal13091316 . hal-04301005

HAL Id: hal-04301005

<https://ulco.hal.science/hal-04301005>





Submitted on 22 Nov 2023

HAL is a multi-disciplinary open access archive for the deposit and dissemination of scientific research documents, whether they are published or not. The documents may come from teaching and research institutions in France or abroad, or from public or private research centers.

L'archive ouverte pluridisciplinaire **HAL**, est destinée au dépôt et à la diffusion de documents scientifiques de niveau recherche, publiés ou non, émanant des établissements d'enseignement et de recherche français ou étrangers, des laboratoires publics ou privés.

Article

Total Catalytic Oxidation of Ethanol over MnCoAl Mixed Oxides Derived from Layered Double Hydroxides: Effect of the Metal Ratio and the Synthesis Atmosphere Conditions

Mariebelle Tannous , Charf Eddine Bounoukta *, Stéphane Siffert , Christophe Poupin  and Renaud Cousin * 

Unité de Chimie Environnementale et Interactions sur le Vivant (UCEIV), Université du Littoral Côte d'Opale, 145 Avenue Maurice Schumann, 59140 Dunkerque, France

* Correspondence: charf-eddine.bounoukta@univ-littoral.fr (C.E.B.); renaud.cousin@univ-littoral.fr (R.C.)

Abstract: In this work, the LDH approach was used to prepare MnCoAl mixed oxides with various textural and structural frameworks for the purpose of enhancing the total oxidation of ethanol. Our results showed that the catalytic activity of the MnCoAl oxides was influenced by the Mn/Co ratio and the gas atmosphere used during synthesis and thermal treatment. Rietveld refinement was processed to estimate the proportion of phases presented in the prepared materials. Our findings indicated that the generation of Mn_2CoO_4 spinel and Mn_5O_8 lamellar phases improved the redox properties and enhanced the active sites in the MnCoAl oxides. Notably, we observed that the catalytic activity at low temperatures of the catalyst increased with the decrease in the cobalt amount. It was also demonstrated that using an N_2 atmosphere during the preparation of the materials is a promising route to prevent the formation of undesirable phases in the LDHs and their corresponding oxides. The presence of an O_2 -free atmosphere during the LDH synthesis positively affects the total ethanol transformation to CO_2 over the oxide catalysts.

Keywords: Mn–Co mixed oxides; layered double hydroxide; ethanol oxidation; synthesis atmosphere



Citation: Tannous, M.; Bounoukta, C.E.; Siffert, S.; Poupin, C.; Cousin, R. Total Catalytic Oxidation of Ethanol over MnCoAl Mixed Oxides Derived from Layered Double Hydroxides: Effect of the Metal Ratio and the Synthesis Atmosphere Conditions. *Catalysts* **2023**, *13*, 1316. <https://doi.org/10.3390/catal13091316>

Academic Editors: Ioan-Cezar Marcu and Octavian Dumitru Pavel

Received: 28 August 2023

Revised: 16 September 2023

Accepted: 20 September 2023

Published: 21 September 2023



Copyright: © 2023 by the authors. Licensee MDPI, Basel, Switzerland. This article is an open access article distributed under the terms and conditions of the Creative Commons Attribution (CC BY) license (<https://creativecommons.org/licenses/by/4.0/>).

1. Introduction

Volatile organic compounds (VOCs) are diverse groups of carbon-based chemicals that exert a significant influence on both air quality and human health [1]. The hydrocarbon pollutants can originate from various sources, including industrial waste, vehicle exhaust, and processes involving solvents and paints. When released into the atmosphere, they contribute to the formation of ground-level ozone, which leads to environmental degradation [2,3]. To address the harmful impact of VOC emissions, heterogeneous catalytic oxidation has emerged as a promising approach. One of the major factors influencing the efficiency of the oxidation process is the choice of catalyst [4].

The most common catalysts used for the total oxidation of VOCs are supported noble metals (platinum, palladium). However, noble metal catalysts are susceptible to poisoning and somewhat costly [5,6]. Therefore, the emphasis is on the development of innovative heterogeneous catalytic materials with low manufacturing costs and high activity at moderate temperatures. In this regard, transition metal oxides are being explored [7].

Mixed oxides may be synthesized using different methods, including co-precipitation, auto-combustion, sol-gel, and hydrothermal procedures, as well as the thermal breakdown of various precursors such as hydroxides, carbonates, and nitrates [8]. One intriguing approach is the layered double hydroxide “LDH” route through metal salts co-precipitation.

LDHs with positively charged metal hydroxide layers and exchangeable interlayer anions offer great advantages in the formation of mixed oxides. The LDH crystallites provide a regulated and tunable framework that facilitates the incorporation of various metal species into the structure [9,10]. LDH-based oxides enable the design of catalysts with

specific compositions, exhibit good textural properties and thermal stability, and may be regenerated numerous times [11]. These materials are becoming more important as catalyst precursors for various industrially important processes, such as methanol-reforming, CO, NO, and VOC emission reduction.

Amongst various oxides employed for VOC abatement, systems including manganese (Mn) and/or cobalt (Co) oxides have exhibited exceptional activity for the total destruction of a wide range of organic molecules, including aromatics, alkanes, and alcohols into CO₂ and H₂O. Manganese and cobalt presence in the same oxide offers a high oxygen storage/release capacity due to their multivalent oxidation states [12]. The catalysts may easily undergo fast reduction–oxidation cycles, making them suitable for VOC oxidation [13–15]. For instance, Dissanayake et al. [16] investigated the impact of the calcination temperature of cobalt oxides on the oxidation of 2-propanol, a representative hazardous alcohol molecule. The highest activity was found in Co₃O₄ calcined at 350 °C, and it was correlated to superior low-temperature reducibility, large pore volumes, higher Co³⁺/Co²⁺ ratios, and abundant active surface oxygen species. In another study conducted by Castaño et al. [17], the effect of different preparation methods of Mn–Co–Mg–Al solids on propanol oxidation was examined. It was illustrated that the co-precipitation of Mn–Co precursors led to the formation of active oxide catalysts with high performances.

Aguilera et al. [18] compared a Cu/Mn/Mg/Al catalyst series with those of Co/Mn/Mg/Al samples in which the Mn/Co or Mn/Cu ratios in the solids were varied from 0 to 0.5. The observed behavior for the ethanol oxidation reaction was related to the development of amorphous phases and redox cycles caused by the cooperative interactions between the active species. The highest Mn/Co proportion exhibits the best catalytic behavior. In Kovanda et al. [19] research work, another class of Co₄Mn_xAl_(2-x) (x = 0–2) mixed oxides catalysts synthesized through the LDH pathway was explored for ethanol oxidation. It was illustrated that the specific activity of the catalysts was promoted when the Mn/Co ratio in the solid phase increased. They also studied the same reaction in another study [20] on Al₂O₃/Al supported Co–Mn–Al mixed oxides, and they showed that increasing the (Mn/Co) ratio improved the catalytic activity in ethanol combustion. This observation has been explained by high reducible component existence.

Moreover, in our recent work [21], we tested the ethanol oxidation over Mn_xMg_(6-x)Al₂O (x = 0–6) catalysts obtained by LDH thermal decomposition. It was established that the ethanol transformation was influenced by the metal ratio, and the Mn₄Mg₂Al₂O catalyst exhibited superior activity compared to the supported metal Pd/γ-Al₂O₃. The presence of manganese species with multiple states in the bulk and on the surface of the materials was shown to be crucial for their activity.

Given this context, this study seeks to investigate the influence of the metal ratio and the synthesis atmosphere on the physicochemical properties and ethanol oxidation catalytic activity of Mn_xCo_(6-x)Al₂ mixed oxides series. To begin with, this work lies in the employment of several characterization techniques such as X-ray diffraction (XRD), N₂ physisorption, and H₂ temperature-programmed reduction (TPR) for the identification and quantification of the different active phases within the catalysts, textural characteristics determination, as well as redox couple properties, respectively. Furthermore, the ethanol conversion and product selectivity are discussed with respect to the physicochemical properties. Finally, the influence of the catalyst synthesis and the thermal treatment atmosphere of the catalysts on the ethanol oxidation performance were assessed.

2. Results

2.1. Catalyst Characterization

The obtained diffraction patterns of the different prepared LDH precursors and their corresponding oxides are shown respectively in Figures 1 and 2. The XRD curves of the samples exhibited the presence of several fragments of different phases. Therefore, Rietveld refinement was processed to assess the approximate weight percentage of the plausibly

suggested phases (Tables 1 and 2). The JCPDS files of the crystalline phases are shown in Figure S1 (Supplementary Materials).

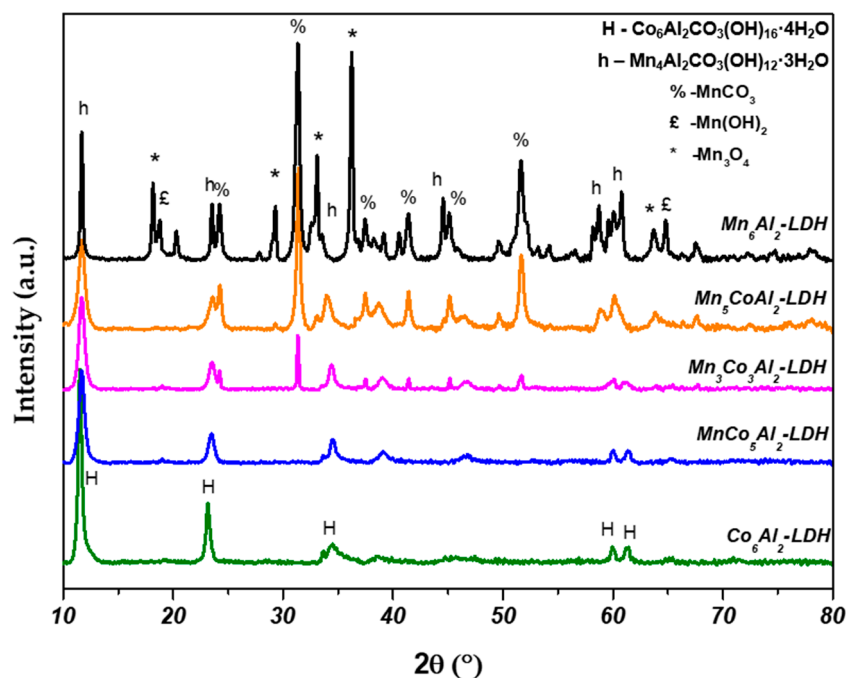


Figure 1. XRD patterns of the different prepared $Mn_xCo_{6-x}Al_2$ -LDH.

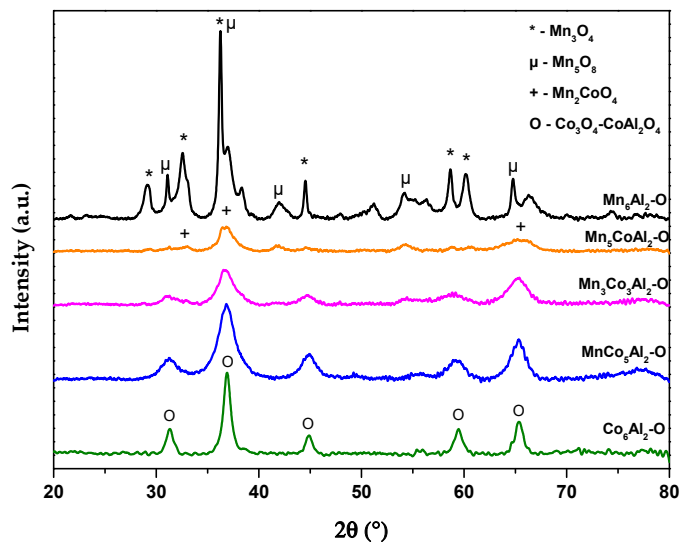


Figure 2. XRD patterns of the different $Mn_xCo_{6-x}Al_2$ mixed oxides.

Table 1. Phase proportions from XRD analysis.

Samples	LDH	MnCO ₃	Mn(OH) ₂	Mn ₂ O ₃	Mn ₃ O ₄
Co ₆ Al ₂ -LDH	100	-	-	-	-
MnCo ₅ Al ₂ -LDH	99.4	0.2	0.4	-	-
Mn ₃ Co ₃ Al ₂ -LDH	82.5	17	0.5	-	-
Mn ₅ CoAl ₂ -LDH	53.4	44.9	-	1.7	-
Mn ₆ Al ₂ -LDH	16.9	48.5	-	0.2	34.4

Table 2. Phases proportion in the different $\text{Mn}_x\text{Co}_{6-x}\text{Al}_2\text{-O}$ mixed oxides obtained after thermal treatment of the LDH from XRD analysis.

Samples	Mn_2CoO_4	Al_2CoO_4	MnAl_2O_4	Mn_2O_3	Mn_3O_4	Mn_5O_8	MnO_2	Co_3O_4
$\text{Co}_6\text{Al}_2\text{-O}$	-	4.6	-	-	-	-	-	95.4
$\text{MnCo}_5\text{Al}_2\text{-O}$	1.3	48.5	11.5	0.2	1.5	1.6	-	35.5
$\text{Mn}_3\text{Co}_3\text{Al}_2\text{-O}$	7.4	62.8	3	-	-	1	3	25.8
$\text{Mn}_5\text{CoAl}_2\text{-O}$	15.5	26.5	-	-	13.5	34.1	10.4	-
$\text{Mn}_6\text{Al}_2\text{-O}$	-	-	27.7	7.6	39.1	24.7	1	-

Concerning the MnCoAl -LDH XRD analysis (Figure 1), the microstructure of the $\text{Co}_6\text{Al}_2\text{-LDH}$ reveals the existence of solely pure hydrotalcite with the chemical formula $\text{Co}_6\text{Al}_2\text{CO}_3(\text{OH})_{16}\cdot 4\text{H}_2\text{O}$ (JCPDS 51-0045). In contrast, the $\text{Mn}_6\text{Al}_2\text{-LDH}$ exhibits a small proportion of $\text{Mn}_4\text{Al}_2\text{CO}_3(\text{OH})_{12}\cdot 3\text{H}_2\text{O}$ (JCPDS 51-1526) LDH phase, known as charmarite, along with a significant amount of manganese carbonate MnCO_3 (JCPDS 44-1472), tetragonal Mn_3O_4 “Hausmannite” (JCPDS 24-0734) and a slight amount of Mn_2O_3 phase (JCPDS 89-4836). In the case of the MnCoAl samples, a similar observation could be made. The subsequent LDH phase was accompanied by the MnCO_3 phase, as well as traces of $\text{Mn}(\text{OH})_2$ (JCPDS 73-1604). Table 1 reports the weight percent of the suggested phases for all samples. For the calculated percent of the LDH phases, the listed values are the sum of both $\text{Co}_6\text{Al}_2\text{CO}_3(\text{OH})_{16}\cdot 4\text{H}_2\text{O}$ and $\text{Mn}_4\text{Al}_2\text{CO}_3(\text{OH})_{12}\cdot 3\text{H}_2\text{O}$ phases.

Overall, it was observed that increasing the Mn content leads to a lower proportion of the LDH phase compared to MnCO_3 , which becomes more pronounced. No matter the Mn loaded in the $\text{Mn}_x\text{Co}_{6-x}\text{Al}_2\text{-LDH}$ sample, it induces octahedral distortion through the Jahn–Teller effect. The big ionic radii size of Mn^{2+} (0.83 Å) affects the coordination environment and prefers a 4:2 coordination with Al^{3+} in the octahedral layer, unlike Co^{2+} (0.74 Å), which only forms the LDH phase. This results in the formation of various Mn phases to accommodate the additional Mn that cannot be incorporated into the lamellar layers of the LDH.

In atmospheric conditions, the auxiliary Mn cations tend to form $\text{Mn}(\text{OH})_2$ brucite in the presence of NaOH. Furthermore, Mn cations may easily precipitate to MnCO_3 at pH = 5 to 11, which is the range of our synthesis conditions [22]. Thus, the remaining $\text{Mn}(\text{OH})_2$ and MnCO_3 in the solution will be easily oxidized by dissolved oxygen from the air to generate Mn_3O_4 , which may later be targeted for further oxidation to form Mn_2O_3 [23–25].

X-ray diffraction (XRD) measurements were carried out on $\text{Mn}_x\text{Co}_{6-x}\text{Al}_2\text{-O}$ samples after the heat treatment of the $\text{Mn}_x\text{Co}_{6-x}\text{Al}_2\text{-LDH}$ precursors in synthetic air at 500 °C (Figure 2). The precursor’s thermal decomposition led to the destruction and collapse of the lamellar structure of the LDH, which resulted in the formation of spinel-type and different metal oxide phases (Table 2).

For the $\text{Co}_6\text{Al}_2\text{-O}$ sample, it could be observed that the pure LDH phase of the binary was almost entirely transformed into Co_3O_4 (JCPDS 65-3103) spinel during the heat treatment, along with a small proportion of Al_2CoO_4 (JCPDS 38-0814) phase. Meanwhile, the $\text{Mn}_6\text{Al}_2\text{-O}$ displayed the presence of monoclinic Mn_5O_8 lamellar phase (JCPDS 39-1218) highly abundant on Mn^{4+} [26], MnAl_2O_4 (JCPDS 29-0880) and various manganese oxide with different proportion. As for the ternary mixed oxides, several phases were formed. However, the increase in the Mn content raises the concentration of the Mn_2CoO_4 phase (JCPDS 77-0471) and MnO_2 (JCPDS 38-0814) within the catalyst’s series.

The $\text{Mn}_3\text{Co}_3\text{Al}_2\text{-O}$ samples revealed the presence of Al_2CoO_4 (JCPDS 38-0814) and Co_3O_4 phases in high proportions. Meanwhile, a moderate concentration of Mn_2CoO_4 phase (7.4%) was observed, along with the presence of MnO_2 and Mn_5O_8 phases. Interestingly, the $\text{Mn}_5\text{CoAl}_2\text{-O}$ displays the formation of a high proportion of Mn_2CoO_4 spinel phase along with a large amount of MnO_2 and Mn_5O_8 phases. This observation suggests the presence of an Mn^{4+} state in the sample.

For the MnCoAl samples, the peak intensity of the tetragonal Co_3O_4 at $2\theta \approx 36^\circ$ was clearly broadened and weakened. These could be due to the formation of a Mn–Co solid solution. The manganese ions can enter the cobalt tetragonal phase and establish an amorphous or crystalline structure. Therefore, this may result in the creation of charge defects and a CoMn synergistic effect, as evidenced by the presence of Mn_2CoO_4 spinel for the Mn_5CoAl sample [27]. It is also important to note that the absence of aluminum oxide phases in Al-rich materials could be attributed to the high dispersion of this element or its presence in an amorphous state.

The porosity parameters of the oxide materials were evaluated and presented in Table 3, and the N_2 adsorption–desorption curves are shown in Figure 3.

Table 3. Textural properties of the $\text{Mn}_x\text{Co}_{6-x}\text{Al}_2\text{O}$ mixed oxides.

Samples	S_{BET} (m^2/g)	Pore Volume (cm^3/g)	Average Pore Size (nm)
$\text{Co}_6\text{Al}_2\text{O}$	110	0.675	20.04
$\text{MnCo}_5\text{Al}_2\text{O}$	154	0.441	10.24
$\text{Mn}_3\text{Co}_3\text{Al}_2\text{O}$	167	0.419	10.16
$\text{Mn}_5\text{CoAl}_2\text{O}$	171	0.373	8.84
$\text{Mn}_6\text{Al}_2\text{O}$	103	0.175	8.78

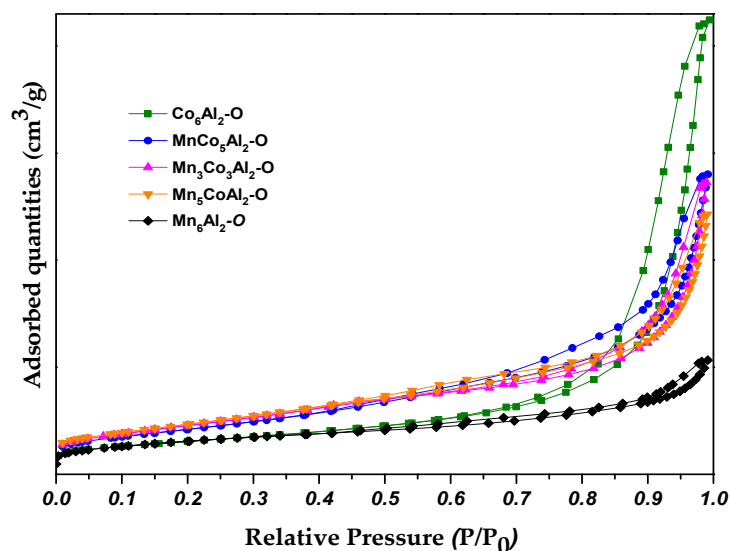


Figure 3. N_2 physisorption isotherms of the $\text{Mn}_x\text{Co}_{6-x}\text{Al}_2\text{O}$ mixed oxides.

All the isotherms of the catalysts exhibited an IV-type behavior with H3-type hysteresis loops (in accordance with the IUPAC), indicating the presence of a mesoporous structure and narrow plate-like particles [28]. The specific surface area of the $\text{Co}_6\text{Al}_2\text{O}$ catalyst was comparable to that of the $\text{Mn}_6\text{Al}_2\text{O}$. Nevertheless, the $\text{Co}_6\text{Al}_2\text{O}$ sample showed a higher pore volume and average pore size in contrast to the $\text{Mn}_6\text{Al}_2\text{O}$ material.

The heat treatment of the co-precipitated precursors, along with the increase in the Mn content in the structure, resulted in a destruction of the octahedral form and interlamellar spacing rearrangement. The LDH structure decomposition leads to the formation of different neighboring aggregates separated by pores of low average diameter.

Interestingly, the specific surface area for the ternary oxides was improved compared to the binary ones. Within the sample series, the surface area was increased while increasing the Mn/Co ratio reversely to the size and volume of the average pores. The Mn presence enhanced the structural disorder that promoted the creation of more pores and changes in the textural properties of the oxide composites [29]. These observations align with the

surface area measurements, which showed that $\text{MnCo}_5\text{Al}_2\text{-O}$ ($154 \text{ m}^2/\text{g}$) presented a lower surface area compared to the $\text{Mn}_5\text{CoAl}_2\text{-O}$ catalyst ($171 \text{ m}^2/\text{g}$).

A general idea of the MnCoAl mixed oxides reducibility was gathered by temperature-programmed reduction (TPR) analysis (Figure 4). For the $\text{Co}_6\text{Al}_2\text{-O}$ sample, the reduction of the spinel phase occurred in two stages at 370°C and 700°C . These temperatures correspond respectively to the $\text{Co}^{3+}/\text{Co}^{2+}$ couple and the complete reduction of Co cations to Co (0) in the spinel phases, as observed by Lou et al. [30]. The TPR profile of the $\text{Mn}_6\text{Al}_2\text{-O}$ catalyst is more complex due to the different oxidation states of manganese species. It could be deconvoluted into four overlapping regions. In relation to the XRD data, it was determined that the peaks labeled A and B are related respectively to the $\text{Mn}^{4+}/\text{Mn}^{3+}$ redox couple of MnO_2 and Mn_5O_8 crystallites in which the phases were totally reduced to Mn_2O_3 . A similar trend was observed in the literature by Lamonier et al. [31]. Indeed, the first reduction peak of MnCoAl catalysts was assigned to the reduction of Mn^{4+} to Mn^{3+} in the lamellar phase.

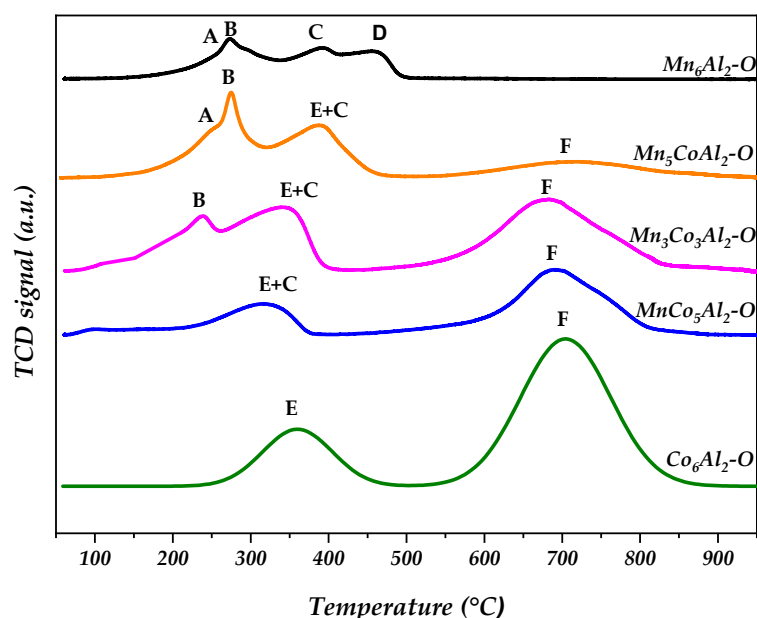


Figure 4. H_2 temperature-programmed reduction (TPR) profiles of the $\text{Mn}_x\text{Co}_{6-x}\text{Al}_2\text{-O}$ mixed oxides.

The peak labeled C is attributed to the reduction of Mn_2O_3 to Mn_3O_4 , and the last reduction step is assigned directly to the destruction of Mn_3O_4 spinel to MnO [18]. Regarding the ternary oxides, the high cobalt ratio in the solid mixture resulted in a TPR curve with two reduction steps similar to that of the $\text{Co}_6\text{Al}_2\text{-O}$ sample. The $\text{Mn}_3\text{Co}_3\text{Al}_2\text{-O}$ sample exhibited three reduction steps, while the $\text{Mn}_5\text{CoAl}_2\text{-O}$ solid displayed four T_{max} summits. This indicates that the redox properties of the ternary oxides are related to the active metal's site concentration. The peak labeled F for the oxide composite catalysts corresponds to the destruction of the different spinel where the Co was totally reduced to form metallic Co. The E+C region for the ternary oxides is assigned to the $\text{Mn}^{3+}/\text{Mn}^{2+}$ and $\text{Co}^{3+}/\text{Co}^{2+}$ reduction couples of the various spinel and Mn_2O_3 phases [32–34].

The second T_{max} peak in the TPR curves of $\text{Mn}_5\text{CoAl}_2\text{-O}$ and $\text{Mn}_3\text{Co}_3\text{Al}_2\text{-O}$ is attributed to the reduction of Mn^{4+} to Mn^{3+} of the layered Mn_5O_8 phase and/or MnO_2 phase while the peak A for $\text{Mn}_5\text{CoAl}_2\text{-O}$ sample could be associated directly to the same couple easily reduced in the spinel Mn_2CoO_4 phase.

In general, the association of Mn along with Co species in a mixed oxide system affects the F region by lowering the reduction temperature and leads to lower H_2 consumption compared to $\text{Co}_6\text{Al}_2\text{-O}$. This is mainly due to the change in the metal–oxygen bond strength in the tetragonal spinels. The Mn–Co synergy in the calcined solids facilitates the reduction of Co cations to metallic Co and the formation of MnO .

Catalysts with a higher quantity of readily reducible components are, in general, more active for VOC abatement. Therefore, the total hydrogen consumption of the different prepared oxides at temperatures lower than 500 °C was recorded (Table 4). The $\text{Mn}_6\text{Al}_2\text{-O}$ sample exhibited more than 50% higher hydrogen consumption compared to the $\text{Co}_6\text{Al}_2\text{-O}$. Moreover, it can be observed that the association of Mn and Co in the MnCoAl materials affects the content of easily reducible species (Mn^{4+} species), as evidenced by an increase in H_2 consumption. The main increase in H_2 consumption is observed for the $\text{Mn}_5\text{CoAl}_2\text{-O}$. This improved reducibility could be explained by the stronger interaction of MnO_x and CoO_x species from the Mn_2CoO_4 spinel phase revealed by XRD. However, the $\text{Mn}_3\text{Co}_3\text{Al}_2\text{-O}$ sample exhibited a significant decrease in the H_2 consumption compared to the $\text{Mn}_5\text{CoAl}_2\text{-O}$ sample. This is mostly due to the presence of a slightly detected amount of Mn^{4+} -rich phases (11.4%), MnO_2 , Mn_5O_8 , and Mn_2CoO_4 .

Table 4. Hydrogen consumption over the $\text{Mn}_x\text{Co}_{6-x}\text{Al}_2\text{-O}$ mixed oxides during the TPR analysis.

Samples	Hydrogen Consumption at T < 500 °C (umol/g)
$\text{Co}_6\text{Al}_2\text{-O}$	3620
$\text{MnCo}_5\text{Al}_2\text{-O}$	3763
$\text{Mn}_3\text{Co}_3\text{Al}_2\text{-O}$	4800
$\text{Mn}_5\text{CoAl}_2\text{-O}$	6110
$\text{Mn}_6\text{Al}_2\text{-O}$	5660

The characterization analysis shows that the Mn/Co ratio has a significant impact on the formed oxides, which could influence the VOCs' oxidation performances. The proportion of the generated phases in the precipitate and their associated oxides are altered by changes in the metal ratio. The findings showed that the surface reducibility and porosity are strongly influenced by the phase composition of the bulk material. The presence of Mn in various oxidation states enables a high oxygen storage capacity within the crystalline lattice [35,36]. In addition, the presence of spinel phases, with their diverse cation composition, plays a crucial role in enhancing the redox properties and the availability of oxygen vacancies. Specifically, when Mn species are in close proximity to cobalt within the same phases, electron exchange interactions between closely coupled pairs of manganese and cobalt facilitate electronic mobility across the surface [27]. Furthermore, the presence of many phases inside a solid structure encourages the formation of a large specific surface area. The large pore sizes and volumes are advantageous during the oxidation process; however, the same could allow the existence of distant segregates that might alter electron density, lowering catalytic activity, which might be the case for the cobalt binary oxide. Another factor that affects VOCs abatement, is the type and form of crystallites. The bidimensional layers of Mn_5O_8 metastable phase, has an abundant interlayer defect with surely one-fourth octahedral oxygen vacancy from the Mn ions site [37]. On the other hand, the Mn_2CoO_4 spinel structure accommodates a mixed-valence oxide form (+2, +3, and +4 o) that obviously increases the catalytic oxidation activity [38].

2.2. Catalytic Activity

2.2.1. Catalytic Oxidation of Ethanol over $\text{Mn}_x\text{Co}_{(6-x)}\text{Al}_2\text{-O}$ Catalysts

The catalytic results of the ethanol total oxidation in the presence of synthetic air over MnCoAl mixed oxides, in terms of conversion, are presented in Figure 5. The light-off curves of all samples exhibit a similar shape, where conversion increased with increasing temperature until total conversion was achieved. The variations in the catalytic activity among the prepared oxides highlight the sensitivity of ethanol oxidation reaction to the Mn/Co-active species in the oxide mixtures. Ethanol transformation was improved greatly after the total substitution of cobalt by manganese. The temperature required for total ethanol conversion T_{100} was shifted to a lower temperature by 38 °C from 200 °C for $\text{Co}_6\text{Al}_2\text{-O}$ to 162 °C for $\text{Mn}_6\text{Al}_2\text{-O}$.

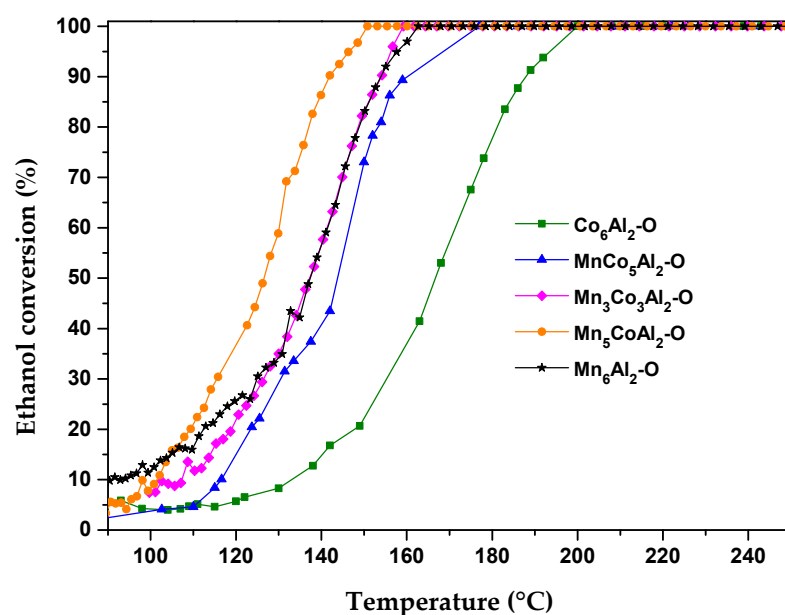


Figure 5. Ethanol conversion curves for $Mn_xCo_{6-x}Al_2-O$ mixed oxides.

The spacing between the interlayers and the abundant unoccupied oxygen sites in the Mn_5O_8 phase in the Mn binary oxide can account for this difference. In addition, it has been observed that the Mn binary oxides contain easily reducible sites with different oxidation states, in contrast to Co -based spinels.

$MnCo_5Al-O$ ternary oxides showed lower oxidation efficiency compared to the Mn_6Al_2-O binary oxides. The separate (M^{3+}/M^{2+}) redox couple of Mn and Co in the spinel phases is slightly less active and requires higher reduction temperatures compared to those found in the binary oxides. Both $Mn_3Co_3Al_2-O$ and Mn_6Al_2-O samples displayed similar catalytic efficiency. Along with the existence of the Mn_2CoO_4 phase, the $Mn_3Co_3Al_2-O$ catalyst possesses high textural properties, which play a crucial role in facilitating the conversion of reactants. Consequently, these characteristics align with the high proportion of the Mn_5O_8 active phase present in the binary oxide.

The optimal reaction behavior for total ethanol oxidation was observed with the Mn_5CoAl_2-O catalyst, which achieved complete ethanol conversion at 152 °C. The sample's improved performance may be attributed mostly to its superior textural-structural features compared to other catalysts. The improved VOC oxidation activity over the Mn_5CoAl_2-O catalyst is attributed to the creation of redox cycles and enhanced porosity resulting from the cooperative action of Mn and Co .

In order to investigate the relationship between catalyst reducibility and ethanol oxidation activity, the T_{50} and the overall hydrogen consumed at temperatures below 500 °C are plotted in Figure 6. The results reveal that a highly readily reducible species on the surface is crucial to achieve sufficient catalytic activity. A huge amount of reducible species results in a considerable decrease in the T_{50} when Mn is present. The T_{50} is reduced by 23 °C for the $MnCo_5Al_2-O$ sample compared to Co_6Al_2-O while increasing hydrogen consumption by less than 4%.

The T_{50} decreases dramatically as the amount of hydrogen employed in the ternary oxide series increases. Meanwhile, the Mn_6Al_2-O sample follows the same linear allocation of the ternary oxides and ranks second, as expected.

The exceptional behavior is revealed for the Mn_5CoAl_2-O catalyst. It can be attributed to the fact that a small amount of Co can stabilize the octahedral layers and modify the surface interaction of Mn^{4+} with ethanol and oxygen molecules.

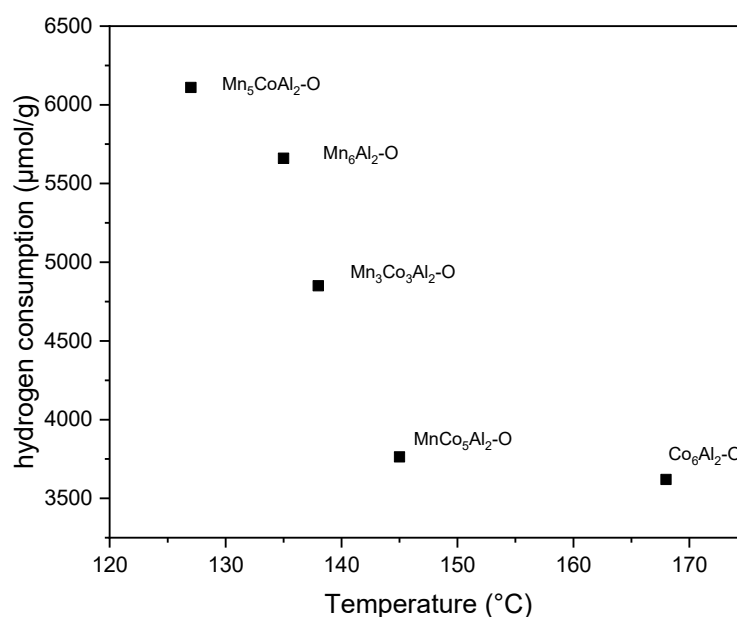
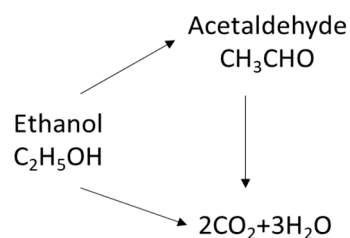


Figure 6. Overall hydrogen consumed at temperatures below 500 °C vs. the T_{50} .

It is well known that ethanol oxidation involves a Mars–van Krevelen mechanism that provides insights into the adsorption and breakdown processes, where metal ions and lattice oxygen play critical roles [38]. Initially, contaminant molecules are adsorbed on the catalyst's surface and oxidized by surface active oxygen species, while transition metal oxides are reduced, creating oxygen vacancies on the surface. Subsequently, the oxygen vacancies are replenished by oxygen from the gas phase, resulting in the reactivation of adsorbed oxygen and the reoxidation of reduced metal oxides [39,40].

It is worth mentioning that the electrical interaction between MnO_x and CoO_x plays an important role in strengthening redox characteristics. The presence of Co^{3+} oxidizes Mn^{2+} to form Co^{2+} and Mn^{3+} . Furthermore, electron transfer occurs between the newly formed Co^{2+} and the existing Mn^{4+} with relatively high surface concentration, promoting the redox cycle: $\text{Co}^{3+}\text{--Mn}^{3+} \leftrightarrow \text{Co}^{2+}\text{--Mn}^{4+}$, which is crucial for catalytic activity following the formation of Co and Mn mixed oxides. Nevertheless, the role of the porosity cannot be neglected. A higher specific area could enhance VOC oxidation activity in the ternary oxides [41,42].

The catalytic oxidation of ethanol yields acetaldehyde as a major reaction intermediate, with CO_2 being the unique product when ethanol is completely oxidized. The carbon balance was nearly total during all the experiments, with only water, CO_2 , and acetaldehyde being the observed products. Despite the presence of hydroxyl groups, ethanol can be completely oxidized to CO_2 or converted to acetaldehyde intermediates, which are then oxidized to CO_2 (Scheme 1) [43].



Scheme 1. Plausible ethanol oxidation reaction mechanism routes [43].

The intermediate acetaldehyde (ACO) product is more hazardous than the original alcohol VOCs. Therefore, it is vital to be aware of the likelihood of partial oxidation products emerging during the catalytic oxidation process [44].

All samples showed a similar trend in terms of detected product selectivity distribution (Figure 7); at low temperatures, acetaldehyde was the predominant product. In contrast, at higher temperatures, CO₂ became the main product. The transformed acetaldehyde amount directly generates the same mole numbers of CO₂ (Figure S2), which means that ethanol activation and transformation are the limiting steps of the oxidation reaction.

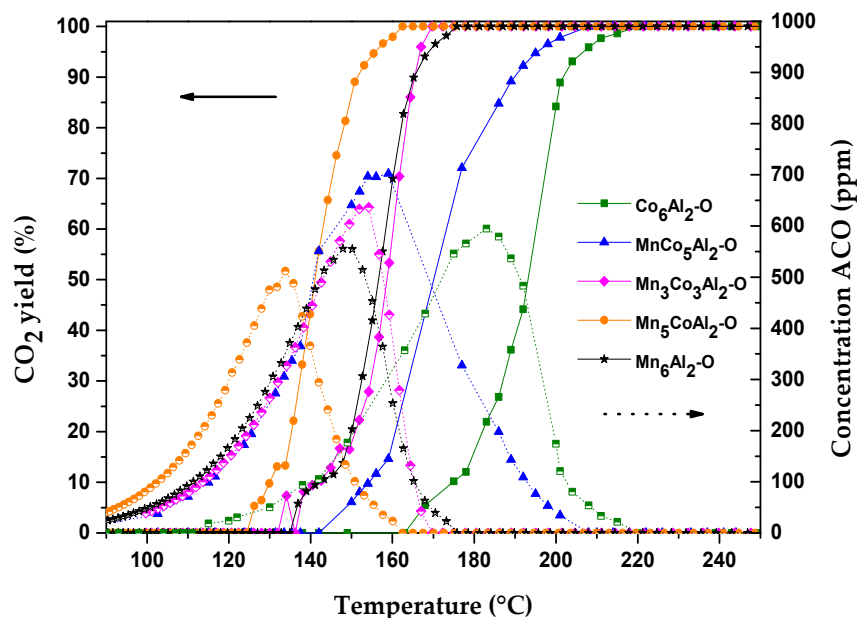


Figure 7. Catalytic oxidation of ethanol over the Mn_xCo_{6-x}Al₂-O mixed oxides: CO₂ yield (solid lines) and acetaldehyde concentration (dotted lines) versus temperature.

Initially, ethanol is transformed to acetaldehyde until a maximum is achieved, and then at temperatures over 120 °C, CO₂ molecules begin to form directly from ethanol or subsequent oxidation of the ensuing acetaldehyde.

The maximum value for the reaction intermediate yield over Mn_xCo_(6-x)Al₂-O catalysts varied from 500 ppm to 700 ppm. It was claimed [44] that the co-precipitation method used for the MnCo mixed oxides preparation leads to high concentrations of acetaldehyde intermediates during the total ethanol transformation by synthetic air. The acetaldehyde selectivity over the different samples significantly changed with the active metals' ratio in the mixed oxides.

The maximum selectivity of acetaldehyde is comparable among the two binary oxides. Nonetheless, a higher temperature is required to totally oxidize the acetaldehyde on Co₆Al₂-O compared to the Mn₆Al₂-O sample (220 °C versus 174 °C). Regarding the ternary oxides, the produced acetaldehyde amount decreased and shifted to lower temperatures with increasing Mn content.

Both O²⁻ anions and mobile oxygen are, respectively, the active sites responsible for ethanol dehydrogenation and acetaldehyde oxidation [45]. The lack of more easily reducible couples for both MnCo₅Al₂-O and Co₆Al₂-O catalysts increased the energy barrier for acetaldehyde production and transformation. Meanwhile, the absence of highly oxidized Mn states from the different detected phases in MnCo₅Al₂-O lowered the rate of further transformation of the intermediate into CO₂, which leads to a maximum generation of acetaldehyde compared to other catalysts.

CO₂ formation over MnCoAl samples follows the order of ethanol conversion. Hence, the assessment of catalyst performance is based on comparing the temperature gap between ethanol conversion and CO₂ yield (Table 5). Overall, as the conversion increases, the temperature gap between the reactant and the final product of ethanol oxidation narrows. At lower conversions, the ΔT in the binary oxides is greater than that of ternary oxides. This could be explained by a larger available surface area, which favors the oxidation of ethanol

and its intermediates. However, towards the end of the oxidation reaction, the temperature gap was influenced by the active sites responsible for ethanol conversion. Over our best catalyst, $\text{Mn}_5\text{CoAl}_2\text{-O}$, the ΔT_{20} was 25 °C and reduced to 13 °C when 50% conversion was accomplished to demonstrate the smallest delay (8 °C) for T_{100} .

Table 5. Comparison of temperature gap between ethanol conversion and CO_2 yields over $\text{Mn}_x\text{Co}_{6-x}\text{Al}_2$ mixed oxides.

Samples	T_{20} (°C)			T_{50} (°C)			T_{100} (°C)		
	Ethanol Conversion	CO_2 Yield	ΔT_{20}	Ethanol Conversion	CO_2 Yield	ΔT_{50}	Ethanol Conversion	CO_2 Yield	ΔT_{100}
$\text{Co}_6\text{Al}_2\text{-O}$	150	190	40	168	192	24	200	220	20
$\text{MnCo}_5\text{Al}_2\text{-O}$	123	160	37	145	170	25	186	210	24
$\text{Mn}_3\text{Co}_3\text{Al}_2\text{-O}$	120	150	30	138	160	22	156	179	23
$\text{Mn}_5\text{CoAl}_2\text{-O}$	110	135	25	127	140	13	152	160	8
$\text{Mn}_6\text{Al}_2\text{-O}$	112	150	38	135	155	20	162	174	12

2.2.2. Effect of the Synthesis and Heat Treatment Atmosphere

For further experimental insights, the influence of the synthesis and heat-treatment conditions was studied in $\text{Mn}_6\text{Al}_2\text{-LDH}$ and $\text{Mn}_5\text{CoAl-LDH}$ samples. Initially, the precipitation of LDH precursors was carried out under a nitrogen atmosphere instead of air ($\text{Mn}_6\text{Al}_2\text{-N}_2\text{-LDH}$, $\text{Mn}_5\text{CoAl}_2\text{-N}_2\text{-LDH}$), and then the obtained solids were calcined under air ($\text{Mn}_6\text{Al}_2\text{-N}_2\text{-O}$ and $\text{Mn}_5\text{CoAl}_2\text{-N}_2\text{-O}$) and under an inert atmosphere ($\text{Mn}_6\text{Al}_2\text{-N}_2\text{-N}_2$ and $\text{Mn}_5\text{CoAl}_2\text{-N}_2\text{-N}_2$). The catalytic performance of the newly tested catalyst series, expressed in terms of CO_2 yield, is presented in Figure 8.

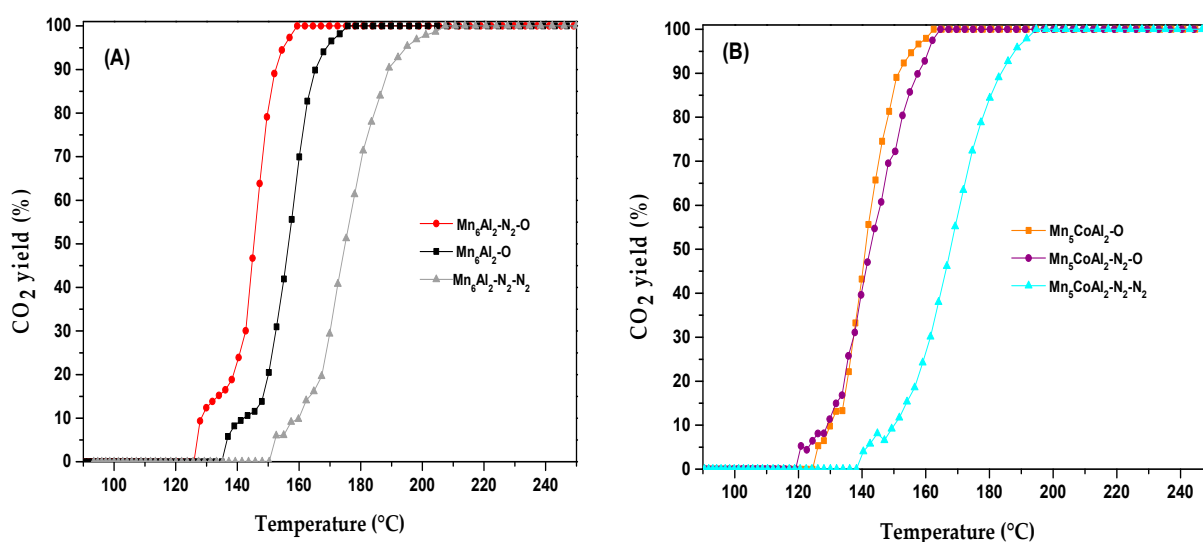


Figure 8. Effect of the synthesis and heat treatment atmosphere for Mn_6Al_2 (A) and Mn_5CoAl_2 (B) catalysts on CO_2 yield.

As observed, ethanol oxidation over catalysts thermally treated under nitrogen ($\text{Mn}_6\text{Al}_2\text{-N}_2\text{-N}_2$ and $\text{Mn}_5\text{CoAl}_2\text{-N}_2\text{-N}_2$) occurred at a higher temperature compared to other catalysts. The temperature of the total ethanol transformation to CO_2 increased by more than 30 °C for the Mn_5CoAl_2 and Mn_6Al_2 samples. The CO_2 yield curves depict that air-calcined binary oxides prepared under nitrogen ($\text{Mn}_6\text{Al}_2\text{-N}_2\text{-O}$) exhibited the lowest temperature for the total degradation of ethanol to carbon dioxide. The change in the synthesis atmosphere in the catalyst preparation seems to involve materials modification, which permits the reduction in the T_{50} of CO_2 yield by 15 °C, from 155 °C for $\text{Mn}_6\text{Al}_2\text{-O}$ to 140 °C for $\text{Mn}_6\text{Al}_2\text{-N}_2\text{-O}$.

The differences observed in the catalytic activity can be explained by the changes in the structural and textural parameters (Table 6). The replacement of the heat treatment gas carrier led to a significant reduction in specific surface area. The predominant phases for the binary and ternary oxides were balanced toward the MnO phase along with a high proportion of the Mn₃O₄ phase.

Table 6. Textural and structural properties of the Mn_xCo_{6-x}Al₂ mixed oxides.

Samples	Textural Properties	Phases Percentage Obtained from XRD								
	S _{BET} (m ² /g)	Mn ₂ CoO ₄	Al ₂ CoO ₄	Mn ₅ O ₈	Mn ₃ O ₄	Mn ₂ O ₃	MnO ₂	Co ₃ O ₄	MnO	MnAl ₂ O ₄
Mn ₆ Al ₂ -O	103	-	-	24.7	39.1	7.6	1	-	-	27.7
Mn ₆ Al ₂ -N ₂ -O	146	-	-	48.9	0.8	25.2	25	-	-	-
Mn ₆ Al ₂ -N ₂ -N ₂	65	-	-	-	33.3	-	-	-	40.3	26.3
Mn ₅ CoAl ₂ -O	171	15.5	26.5	34.1	13.5	-	10.4	-	-	-
Mn ₅ CoAl ₂ -N ₂ -O	189	46.9	31.6	0.5	-	3.3	-	16.7	-	1
Mn ₅ CoAl ₂ -N ₂ -N ₂	114	5.7	21.6	0.8	26.7	1	1	2.3	39	1.8

For the Mn₆Al₂-N₂-O sample, prepared under nitrogen and heat-treated under air, XRD data (Table 6, Figure S3) reveals that the proportion of Mn₅O₈ was increased while the Mn₃O₄ phase almost completely disappeared, with the formation of a significant amount of MnO₂ (25%). The synthesis of the Mn₅CoAl₂-N₂-O material under the N₂ atmosphere hinders the formation of the Mn₃O₄ spinel phase. It can also be seen that the amount of the lamellar phase Mn₅O₈ is negligible, while the percentage of Mn₂CoO₄ spinel was increased by nearly three times.

Thus, it can be assumed that a higher proportion of lamellar Mn₅O₈ in the structure enhances the specific area and the amount of oxygen vacancies. This led to an improvement in the catalytic activity of the Mn₆Al₂-N₂-O sample. However, for Mn₅CoAl₂-N₂-O, the increase in the Mn₂CoO₄ fraction had no significant influence on the catalytic activity. The inclusion of the spinel phase stipulated a slight improvement in activity at low reaction temperatures. In contrast, at higher temperatures, the presence of less amount of Mn⁴⁺ containing phases along with the exitance of Co₃O₄ active phase is expected to decrease the catalytic performance for the Mn₅CoAl₂-N₂-O sample.

The presence of nitrogen during the LDH structure formation may also impact the structural characteristics and hence is accountable for the change in the final obtained calcined materials. The crystallite phases formed in the catalyst series were investigated in Figure S4, and their corresponding percentages are listed in Table 7.

Table 7. Proportion of the different phases of LDH samples from XRD analysis.

Samples	LDH	MnCO ₃	Mn(OH) ₂	Mn ₂ O ₃	Mn ₃ O ₄
Mn ₆ Al ₂ -LDH	16.9	48.5	-	0.2	34.4
Mn ₆ Al ₂ -N ₂ -LDH	54.2	43	-	2.6	0.2
Mn ₅ CoAl ₂ -LDH	53.4	44.9	-	1.7	-
Mn ₅ CoAl ₂ -N ₂ -LDH	62	35.4	-	2.6	-

The use of nitrogen as a carrier gas atmosphere promotes the development of the LDH phase while decreasing the formation of metal carbonates. The use of an inert environment prevented Mn segregation into oxide and hydroxide during salt co-precipitation. These findings emphasize the significance of removing undesired phases and provide fresh insight into the synthesis processes and their influence on the physicochemical parameters and catalytic performance of MnCoAl-based oxide catalysts for VOC abatement.

From all the above, it becomes evident that the percentage of Mn⁴⁺-based phases significantly affects the catalytic ethanol oxidation. A relationship between T₅₀ of CO₂ yield and the sum of Mn⁴⁺-based phases (Mn₂CoO₄, MnO₂, and Mn₅O₈) percentages is

presented in Figure 9. A clear correlation is revealed between the percentage of Mn^{4+} -based phases and T_{50} , especially when the proportion is less than 50%. The temperature at which ethanol reaches half conversion decreases dramatically, from 175 °C in the case of $\text{Mn}_6\text{Al}_2\text{-N}_2\text{-N}_2$ to 135 °C for the $\text{Mn}_5\text{CoAl}_2\text{-N}_2\text{-O}$ sample. This result highlights the important fact that ethanol conversion is directly related to the availability of Mn^{4+} , regardless of whether Co is present alongside Mn. Apparently, the results reveal that for more than 45% of highly Mn-active phases, T_{50} does not change significantly. This is mainly due to the saturation of free available sites, making ethanol oxidation activity independent of the Mn^{4+} content at higher proportions.

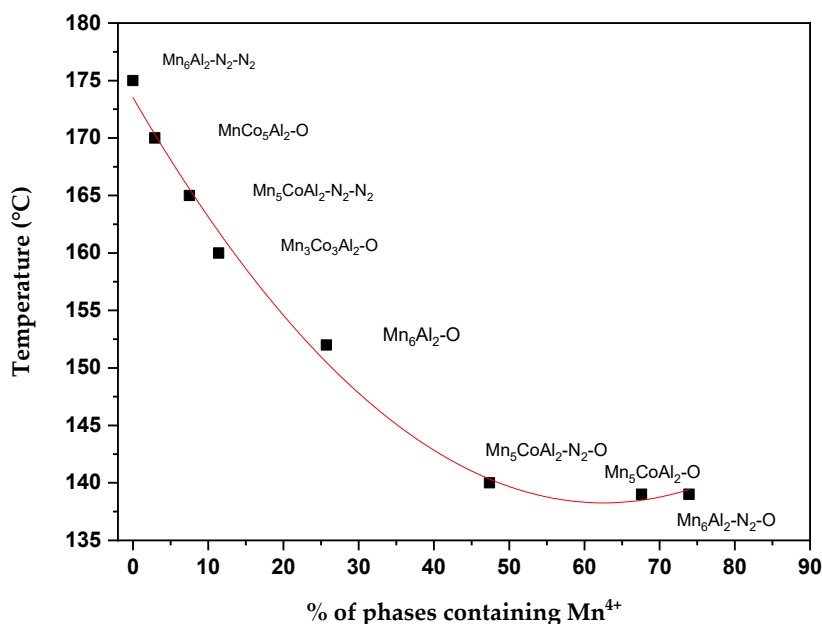


Figure 9. The relationship between T_{50} (°C) and the sum of phase percentages containing Mn^{4+} .

In order to compare the efficiency of these catalysts, Table 8 reports several literature data (T_{50} and T_{100}) for various Mn- and/or Co-based oxides catalysts investigated for the complete ethanol oxidation to CO_2 . Despite differences in operating conditions, our best catalysts demonstrated exceptionally high activity under mild reaction conditions with relatively low pollutant concentrations. The superior catalytic activity of $\text{Mn}_5\text{CoAl}_2\text{-O}$ and $\text{Mn}_6\text{Al}_2\text{-N}_2\text{-O}$ can be attributed to the presence of a substantial number of $\text{Mn}^{4+}/\text{Mn}^{3+}$ redox pairs, along with a high surface area, compared to the other reported catalysts. Under identical experimental conditions, the prepared samples outperformed our previously investigated $\text{Mn}_4\text{Mg}_2\text{Al}_2\text{-O}$ catalyst. At the initial reduction steps, the Mn_5CoAl_2 material showed the presence of easily reducible manganese species.

From this table, it is evident that ethanol conversion is related to both the total flow rate and ethanol concentration. The Cu–Co–Mn exhibited a low T_{50} for ethanol oxidation compared to our catalysts, which can be attributed to a lower total flow rate. Similar results were observed with the Mn_1Co_1 sample, where total ethanol oxidation occurred at a relatively low temperature of 120 °C compared to the other mentioned catalysts. Interestingly, the produced quantity of the undesirable intermediate ACO over Mn_1Co_1 was 100%, which is twice the amount obtained when using Mn_5CoAl_2 as a catalyst for the total ethanol conversion to CO_2 .

On the other hand, the T_{100} of ethanol over $\text{CoMn}_{0.5}$ was approximately 252 °C, despite using double the mass of the catalyst compared to our conditions and even though the sample presented the highest BET surface area among other reported catalysts. This is mainly due to the high flow rate of the gas inlet.

Table 8. Catalytic efficiency of various Mn/Co oxide catalysts in ethanol oxidation.

Catalyst	Experimental Conditions				Catalytic Results		
	Catalyst Mass (mg)	[Ethanol] (ppm)	Flow Rate (mL/min)	S _{BET} (m ² /g)	T ₅₀ (°C)	T ₁₀₀ (°C)	References
Cu–Co–Mn	100	750	33	62	105	173	[44]
Co ₄ MnAl	750	530	125	93	155	192	[45]
Mn ₉ Cu ₁	300	1000	100	30	125	185	[46]
MnO _x /Al ₂ O ₃	300	500	100	103	200	240	[47]
CoMn _{0.5}	200	100	200	249	198	252	[18]
Mn ₄ Mg ₂ Al ₂ –O	100	1000	100	108	156	210	[21]
Mn ₁ Co ₁	100	300	100	208	80	120	[48]
Mn ₅ CoAl ₂ –O	100	1000	100	171	140	160	This work
Mn ₆ Al ₂ –N ₂ –O	100	1000	100	146	142	152	This work

3. Materials and Methods

3.1. Catalysts Preparation

The samples with varying Co and Mn contents were synthesized using a co-precipitation method: Mn_xCo_{6–x}Al₂–LDH with $x = 0–6$ with theoretical molar ratios of 3:2. An aqueous solution containing the required amount of divalent cations in the form of cobalt (II) nitrates Co(NO₃)₂·3H₂O (Thermo Fisher Scientific, IIRKIRCH CEDEX, France, 97%) or manganese (II) nitrates Mn(NO₃)₂·6H₂O (Thermo Fisher Scientific, IIRKIRCH CEDEX, France, 97.5%) and trivalent cations in the form of aluminum (III) nitrates Al(NO₃)₃·9H₂O (1 M, Thermo Fisher Scientific, IIRKIRCH CEDEX, France, 99.5%). By steadily adding a weak solution of NaOH (2 M, Sigma Aldrich, St-Quentin-Fallavier Cedex, France, 98%), the pH was maintained at 9.5. After complete addition, the solution was stirred overnight at room temperature, which is known as the maturation phase, during which the LDH crystallization is assured gradually. The solids were then filtered and washed multiple times with hot deionized water (60 °C) to remove Na⁺ ions, then dried at 60 °C. The dried solids, therefore, were ground in a mortar and then calcined at 500 °C (1 °C min^{–1}) for 4 h to obtain the required mixed oxides. The obtained LDHs are named like Mn_{6–x}Co_xAl₂–LDH where $x = 0, 1$, or 3 , and the mixed oxides obtained after calcination are denoted Mn_{6–x}Co_xAl₂–O.

The synthesis of the samples under nitrogen was conducted using a sealed reactor, where nitrogen gas was passed through a spiral tube at the center of the reactor before the synthesis in order to purge the reactor and during the synthesis to maintain the inert atmosphere. Only a small hole was opened to add the NaOH solution and allow the gas to exit the reactor. The co-precipitation method described earlier was employed, and the resulting solutions were filtered, washed, and dried in the reactor, which was traversed by an inert gas flow and immersed in an oil bath at 60 °C. The obtained LDHs were subsequently treated under air (Mn₆Al₂–N₂–O, Mn₅CoAl₂–O) and inert atmosphere (Mn₆Al₂–N₂–N₂, Mn₅CoAl₂–N₂–O).

3.2. Catalysts Characterization

The crystallinity of the materials was assessed at room temperature using a Bruker D8 Advance diffractometer (Bruker AXS, Billerica, MA, USA) equipped with a CuK copper anode ($\lambda = 1.5406$), a secondary monochromator, and a LynxEye detector to record X-ray diffractograms. For all samples, scattering intensities were measured across an angular range of 10° to 80° for LDH samples and 20° to 80° for oxides with a $2\theta = 0.02^\circ$ measurement step and a 2 s integration time. The diffraction patterns were indexed by comparing them to the ICDD's (International Center for Diffraction Data) "Joint Committee on Powder Diffraction Standards" (JCPDS) files. The phase abundance percentages in the solids were obtained by the Rietveld refinement of multiphase systems performed with MAUD (Materials Analysis Using Diffraction) software '2.998 version', which uses the basic model to calculate the theoretical powder diffraction scheme based on fundamental crystallographic principles. The software considers factors such as the symmetry of the

cell parameters, crystal symmetry, and atomic diffusion factors. MAUD iteratively adjusts the crystallographic parameters of the original model in order to minimize the difference between the calculated theoretical model and the experimental data. This minimization approach seeks to obtain the best fit between observed and calculated diffraction diagrams.

The number of iterations continues until convergence is reached, which indicates that the refined parameters provide a better representation of the crystalline structure. The textural properties were assessed using a Micromeritics VacPrep 061 degasser and physisorption of nitrogen (Micromeritics, Norcross, GA, USA). The sample is pretreated at 350 °C for 4 h under vacuum before each analysis. The specific surface area was calculated by the Brunauer–Emmett–Teller (BET) model, while the Barrett–Joyner–Halenda (BJH) model was used to determine the pore diameter and specific pore volume. H₂ temperature-programmed reduction (H₂-TPR) experiments were performed using a Micromeritics AutoChem II 2920 Version Instrument (Micromeritics, Norcross, GA, USA) equipped with a TCD detector.

The mixed oxide catalyst was first treated at 150 °C with Ar flow. Once cooled down, the sample was subjected to a mixture of 10% H₂/Ar gas at a flow rate of 50 mL/min, with a heating rate of 10 °C/min from room temperature to 950 °C.

3.3. Catalytic Measurements

At atmospheric pressure, the activity of the catalyst, used in powdered form (100 mg), was monitored in a continuous-flow U-glass reactor placed in a tube furnace at a predetermined temperature.

The reactant gas was composed of 1000 ppm of gaseous ethanol balanced with synthetic air (20% O₂ + balance N₂) with less than 5 ppm of water, which was introduced into the reactor at a continuous flow of 100 mL min^{−1}.

The catalyst (100 mg) was pretreated for 1 h at 350 °C in air (33 mL min^{−1}). This allows for the removal of absorbed water and physisorbed organic contaminants that might clog active surface areas. Before doing the catalytic tests, blanks were performed concurrently with catalyst activation to ensure a steady initial reaction mixture (Bypass direction). After activation, the reactant gas passed through the catalyst bed, and the tests were conducted with a temperature drop starting from 300 °C to 90 °C in order to avoid possible adsorption phenomena that could occur at low temperatures. The outlet gas stream concentrations were analyzed by a micro-gas chromatograph CP-4900 (Agilent Technologies Inc., Santa Clara, CA, USA).

The data collected can be used to calculate the conversions of the reactant $X(T)$, the selectivity's $Sp(T)$, and the yield of the products $Y(T)$, which are specified for each temperature T by the following relationships:

$$\begin{aligned}\text{Ethanol conversion : } X(T) &= \frac{C_{i,\text{in}} - C_{i,\text{out}}}{C_{i,\text{in}}} \\ \text{Selectivity : } Sp(T) &= \frac{C_{p,\text{out}}}{\sum C_{p,\text{out}}} \\ \text{Yield : } Y(T) &= X(T) \times Sp(T)\end{aligned}$$

where $C_{i,\text{in}}$ represents the concentration of reactant fed to the reactor, and $C_{i,\text{out}}$ and $C_{p,\text{out}}$ represent the concentrations of the reactant and product in the outlet stream, respectively.

4. Conclusions

A co-precipitation method was used to successfully prepare MnCoAl mixed metal oxides using the LDH approach. Changes in the Mn/Co ratio led to structural and porosity variations in LDH and their resulting oxides. The addition of manganese in ternary oxide increases the defects in the catalyst structure, resulting in textural and structural modifications. The presence of Mn₂CoO₄ spinel and Mn₅O₈ lamellar phases in the Mn₅CoAl₂-O is beneficial since they contribute significantly to catalytic activity. Furthermore, the choice of gas carrier during precipitate preparation and heat treatment influences the total ethanol oxidation process. Mixed oxides with a great number of highly reducible species, larger

specific surface areas, and a higher Mn/Co synergy species exhibited superior performance. Our best catalysts, $\text{Mn}_5\text{CoAl}_2\text{-O}$ and $\text{Mn}_6\text{Al}_2\text{-N}_2\text{-O}$, achieved complete ethanol conversion to CO_2 at low temperatures (160°C). $\text{Mn}_5\text{CoAl}_2\text{-O}$ not only enhances ethanol conversion but also effectively controls the formation of acetaldehyde intermediates and converts them completely to CO_2 at lower temperatures. This work provides a good insight for controlling the LDH crystallite growth and govern the generation of the desired phases in MnCoAl mixed oxides to eliminate ethanol VOCs at lower temperatures.

Supplementary Materials: The following supporting information can be downloaded at <https://www.mdpi.com/article/10.3390/catal13091316/s1>, Figure S1: JCPDS files of the identified phases; Figure S2: Products selectivity of the ethanol oxidation over $\text{Mn}_x\text{Co}_{6-x}\text{Al}_2$ mixed oxides catalysts; Figure S3: XRD patterns of the $\text{Mn}_x\text{Co}_{6-x}\text{Al}_2\text{-O}$ ($x = 6$ or 5) mixed oxides, effect of the heat treatment atmosphere; Figure S4: XRD patterns of the $\text{Mn}_x\text{Co}_{6-x}\text{Al}_2\text{-LDH}$ ($x = 6$ or 5) LDH, effect of the synthesis atmosphere.

Author Contributions: M.T.: experiment validation, data acquisition and treatment, writing—original draft preparation. C.E.B.: data curation, formal analysis, writing—reviewing and editing the original draft. S.S.: conceptualization, visualization, and supervision. C.P.: writing—reviewing and editing the original draft, methodology, conceptualization, and supervision. R.C.: methodology, funding acquisition, project administration, supervision, and final manuscript revision. All authors have read and agreed to the published version of the manuscript.

Funding: The authors would like to express their gratitude to the “Dépollutair” (Interreg V France-Wallonie-Vlaanderen) and “COVO” (CPER-IRENE) projects for their financial support of this research.

Data Availability Statement: The data that support the findings of this study are available from the corresponding author upon reasonable request.

Acknowledgments: M. Tannous thanks the Région Hauts-de-France and the Pôle Métropolitain de la Côte d’Opale for the Ph.D. grant.

Conflicts of Interest: The authors declare no conflict of interest.

References

- Williams, J.; Koppmann, R. Volatile Organic Compounds in the Atmosphere: An Overview. In *Volatile Organic Compounds in the Atmosphere*; John Wiley & Sons, Ltd.: Hoboken, NJ, USA, 2007; pp. 1–32, ISBN 978-0-470-98865-7.
- Khan, F.I.; Ghoshal, A.K. Removal of Volatile Organic Compounds from Polluted Air. *J. Loss Prev. Process. Ind.* **2000**, *13*, 527–545. [CrossRef]
- Jenkin, M.E.; Derwent, R.G.; Wallington, T.J. Photochemical Ozone Creation Potentials for Volatile Organic Compounds: Rationalization and Estimation. *Atmos. Environ.* **2017**, *163*, 128–137. [CrossRef]
- Kuśtrowski, P.; Rokicińska, A.; Kondratowicz, T. Chapter Nine—Abatement of Volatile Organic Compounds Emission as a Target for Various Human Activities Including Energy Production. In *Advances in Inorganic Chemistry*; van Eldik, R., Macyk, W., Eds.; Materials for Sustainable Energy; Academic Press: Cambridge, MA, USA, 2018; Volume 72, pp. 385–419.
- Liu, Y.; Deng, J.; Xie, S.; Wang, Z.; Dai, H. Catalytic Removal of Volatile Organic Compounds Using Ordered Porous Transition Metal Oxide and Supported Noble Metal Catalysts. *Chin. J. Catal.* **2016**, *37*, 1193–1205. [CrossRef]
- Liotta, L.F. Catalytic Oxidation of Volatile Organic Compounds on Supported Noble Metals. *Appl. Catal. B Environ.* **2010**, *100*, 403–412. [CrossRef]
- Campesti, M.A.; Mariani, N.J.; Pramparo, M.C.; Barbero, B.P.; Cadús, L.E.; Martínez, O.M.; Barreto, G.F. Combustion of Volatile Organic Compounds on a MnCu Catalyst: A Kinetic Study. *Catal. Today* **2011**, *176*, 225–228. [CrossRef]
- Bezerra, D. Influence of the Preparation Method on the Structural Properties of Mixed Metal Oxides. *Sci. Technol. Mater.* **2018**, *30*, 166–173. [CrossRef]
- Debecker, D.P.; Gaigneaux, E.M.; Busca, G. Exploring, Tuning, and Exploiting the Basicity of Hydrotalcites for Applications in Heterogeneous Catalysis. *Chem. Eur. J.* **2009**, *15*, 3920–3935. [CrossRef]
- Theiss, F.L.; Ayoko, G.A.; Frost, R.L. Synthesis of Layered Double Hydroxides Containing Mg^{2+} , Zn^{2+} , Ca^{2+} and Al^{3+} Layer Cations by Co-Precipitation Methods—A Review. *Appl. Surf. Sci.* **2016**, *383*, 200–213. [CrossRef]
- Jijoe, P.S.; Yashas, S.R.; Shivaraju, H.P. Fundamentals, Synthesis, Characterization and Environmental Applications of Layered Double Hydroxides: A Review. *Environ. Chem. Lett.* **2021**, *19*, 2643–2661. [CrossRef]
- Mitrani, G.; Chen, S.; Seo, D.-K. Role of Oxygen Vacancies and $\text{Mn}^{4+}/\text{Mn}^{3+}$ Ratio in Oxidation and Dry Reforming over Cobalt-Manganese Spinel Oxides. *Mol. Catal.* **2020**, *483*, 110704. [CrossRef]

13. Bastos, S.S.T.; Órfão, J.J.M.; Freitas, M.M.A.; Pereira, M.F.R.; Figueiredo, J.L. Manganese Oxide Catalysts Synthesized by Exotemplating for the Total Oxidation of Ethanol. *Appl. Catal. B Environ.* **2009**, *93*, 30–37. [\[CrossRef\]](#)
14. Ludvíková, J.; Jiráťová, K.; Klempa, J.; Boehmová, V.; Obalová, L. Titania Supported Co–Mn–Al Oxide Catalysts in Total Oxidation of Ethanol. *Catal. Today* **2012**, *179*, 164–169. [\[CrossRef\]](#)
15. Santos, V.P.; Pereira, M.F.R.; Órfão, J.J.M.; Figueiredo, J.L. The Role of Lattice Oxygen on the Activity of Manganese Oxides towards the Oxidation of Volatile Organic Compounds. *Appl. Catal. B Environ.* **2010**, *99*, 353–363. [\[CrossRef\]](#)
16. Dissanayake, S.; Wasalathanthri, N.; Shirazi Amin, A.; He, J.; Poges, S.; Rathnayake, D.; Suib, S.L. Mesoporous Co₃O₄ Catalysts for VOC Elimination: Oxidation of 2-Propanol. *Appl. Catal. Gen.* **2020**, *590*, 117366. [\[CrossRef\]](#)
17. Castaño, M.; Molina, R.; Moreno, S. Cooperative Effect of the Co–Mn Mixed Oxides for the Catalytic Oxidation of VOCs: Influence of the Synthesis Method. *Appl. Catal. Gen.* **2015**, *492*, 48–59. [\[CrossRef\]](#)
18. Aguilera, D.A.; Perez, A.; Molina, R.; Moreno, S. Cu–Mn and Co–Mn Catalysts Synthesized from Hydrotalcites and Their Use in the Oxidation of VOCs. *Appl. Catal. B Environ.* **2011**, *104*, 144–150. [\[CrossRef\]](#)
19. Kovanda, F.; Rojka, T.; Dobešová, J.; Machovič, V.; Bezdička, P.; Obalová, L.; Jiráťová, K.; Grygar, T. Mixed Oxides Obtained from Co and Mn Containing Layered Double Hydroxides: Preparation, Characterization, and Catalytic Properties. *J. Solid State Chem.* **2006**, *179*, 812–823. [\[CrossRef\]](#)
20. Kovanda, F.; Jiráťová, K.; Ludvíková, J.; Raabová, H. Co–Mn–Al Mixed Oxides on Anodized Aluminum Supports and Their Use as Catalysts in the Total Oxidation of Ethanol. *Appl. Catal. Gen.* **2013**, *464–465*, 181–190. [\[CrossRef\]](#)
21. El Khawaja, R.; Rochard, G.; Genty, E.; Poupin, C.; Siffert, S.; Cousin, R. Optimization of Mn–Mg–Al Mixed Oxides Composition on Their Activity towards the Total Oxidation of Aromatic and Oxygenated VOCs. *Eur. J. Inorg. Chem.* **2023**, *26*, e202300213. [\[CrossRef\]](#)
22. Tian, Z.-Y.; Ngamou, P.; Vannier, V.; Kohse-Höinghaus, K. Catalytic Oxidation of VOCs over Mixed Co–Mn Oxides. *Appl. Catal. B Environ.* **2012**, *117–118*, 125–134. [\[CrossRef\]](#)
23. Gennequin, C.; Siffert, S.; Cousin, R.; Aboukais, A. Co–Mg–Al Hydrotalcite Precursors for Catalytic Total Oxidation of Volatile Organic Compounds. *Top. Catal.* **2009**, *52*, 482–491. [\[CrossRef\]](#)
24. Obalová, L.; Pacultová, K.; Balabánová, J.; Jiráťová, K.; Bastl, Z.; Valášková, M.; Lacný, Z.; Kovanda, F. Effect of Mn/Al Ratio in Co–Mn–Al Mixed Oxide Catalysts Prepared from Hydrotalcite-like Precursors on Catalytic Decomposition of N₂O. *Catal. Today* **2007**, *119*, 233–238. [\[CrossRef\]](#)
25. Klyushina, A.; Pacultová, K.; Karásková, K.; Jiráťová, K.; Ritz, M.; Fridrichová, D.; Volodarskaja, A.; Obalová, L. Effect of Preparation Method on Catalytic Properties of Co–Mn–Al Mixed Oxides for N₂O Decomposition. *J. Mol. Catal. Chem.* **2016**, *425*, 237–247. [\[CrossRef\]](#)
26. Jeong, D.; Jin, K.; Jerng, S.E.; Seo, H.; Kim, D.; Nahm, S.H.; Kim, S.H.; Nam, K.T. Mn₅O₈ Nanoparticles as Efficient Water Oxidation Catalysts at Neutral pH. *ACS Catal.* **2015**, *5*, 4624–4628. [\[CrossRef\]](#)
27. Tang, W.; Wu, X.; Li, S.; Li, W.; Chen, Y. Porous Mn–Co Mixed Oxide Nanorod as a Novel Catalyst with Enhanced Catalytic Activity for Removal of VOCs. *Catal. Commun.* **2014**, *56*, 134–138. [\[CrossRef\]](#)
28. Aisawa, S.; Hirahara, H.; Uchiyama, H.; Takahashi, S.; Narita, E. Synthesis and Thermal Decomposition of Mn–Al Layered Double Hydroxides. *J. Solid State Chem.* **2002**, *167*, 152–159. [\[CrossRef\]](#)
29. Mo, S.; Li, S.; Li, W.; Li, J.; Chen, J.; Chen, Y. Excellent Low Temperature Performance for Total Benzene Oxidation over Mesoporous CoMnAl Compositized Oxides from Hydrotalcites. *J. Mater. Chem. A* **2016**, *4*, 8113–8122. [\[CrossRef\]](#)
30. Lou, Y.; Wang, L.; Zhao, Z.; Zhang, Y.; Zhang, Z.; Lu, G.; Guo, Y.; Guo, Y. Low-Temperature CO Oxidation over Co₃O₄-Based Catalysts: Significant Promoting Effect of Bi₂O₃ on Co₃O₄ Catalyst. *Appl. Catal. B Environ.* **2014**, *146*, 43–49. [\[CrossRef\]](#)
31. Boyero Macstre, J.; Fernández López, E.; Gallardo-Amores, J.M.; Ruano Casero, R.; Sánchez Escribano, V.; Pérez Bernal, E. Influence of Tile Synthesis Parameters on the Structural and Textural Properties of Precipitated Manganese Oxides. *Int. J. Inorg. Mater.* **2001**, *3*, 889–899. [\[CrossRef\]](#)
32. Li, L.; Liu, Y.; Liu, J.; Zhou, B.; Guo, M.; Liu, L. Catalytic Degradation of Toluene over MnO₂/LaMnO₃: Effect of Phase Type of MnO₂ on Activity. *Catalysts* **2022**, *12*, 1666. [\[CrossRef\]](#)
33. Li, G.; Li, N.; Sun, Y.; Qu, Y.; Jiang, Z.; Zhao, Z.; Zhang, Z.; Cheng, J.; Hao, Z. Efficient Defect Engineering in Co–Mn Binary Oxides for Low-Temperature Propane Oxidation. *Appl. Catal. B Environ.* **2021**, *282*, 119512. [\[CrossRef\]](#)
34. Bulavchenko, O.A.; Gerasimov, E.Y.; Afonasenkov, T.N. Reduction of Double Manganese–Cobalt Oxides: In Situ XRD and TPR Study. *Dalton Trans.* **2018**, *47*, 17153–17159. [\[CrossRef\]](#) [\[PubMed\]](#)
35. Zhao, H.; Wang, H.; Qu, Z. Synergistic Effects in Mn–Co Mixed Oxide Supported on Cordierite Honeycomb for Catalytic Deep Oxidation of VOCs. *J. Environ. Sci.* **2022**, *112*, 231–243. [\[CrossRef\]](#)
36. Shah, P.M.; Bailey, L.A.; Taylor, S.H. The Influence of Cerium to Manganese Ratio and Preparation Method on the Activity of Ceria–Manganese Mixed Metal Oxide Catalysts for VOC Total Oxidation. *Catalysts* **2023**, *13*, 114. [\[CrossRef\]](#)
37. Zlatanova, Z.; Marinova, D.; Kukeva, R.; Mihaylov, L.; Nihtianova, D.; Stoyanova, R. Layered Manganese Oxide Mn₅O₈ as a Structural Matrix for Fast Lithium and Magnesium Intercalation. *J. Alloys Compd.* **2021**, *851*, 156706. [\[CrossRef\]](#)
38. Ren, Y.; Qu, Z.; Wang, H.; Zhao, A. Acid-Etched Spinel CoMn₂O₄ with Highly Active Surface Lattice Oxygen Species for Significant Improvement of Catalytic Performance of VOCs Oxidation. *Chem. Eng. J.* **2023**, *463*, 142316. [\[CrossRef\]](#)

39. Morales, M.R.; Yeste, M.P.; Vidal, H.; Gatica, J.M.; Cadus, L.E. Insights on the Combustion Mechanism of Ethanol and N-Hexane in Honeycomb Monolithic Type Catalysts: Influence of the Amount and Nature of Mn-Cu Mixed Oxide. *Fuel* **2017**, *208*, 637–646. [\[CrossRef\]](#)
40. Doornkamp, C.; Poncet, V. The Universal Character of the Mars and Van Krevelen Mechanism. *J. Mol. Catal. Chem.* **2000**, *162*, 19–32. [\[CrossRef\]](#)
41. Luo, Y.; Zheng, Y.; Zuo, J.; Feng, X.; Wang, X.; Zhang, T.; Zhang, K.; Jiang, L. Insights into the High Performance of Mn-Co Oxides Derived from Metal-Organic Frameworks for Total Toluene Oxidation. *J. Hazard. Mater.* **2018**, *349*, 119–127. [\[CrossRef\]](#)
42. Bratan, V.; Vasile, A.; Chesler, P.; Hornoiu, C. Insights into the Redox and Structural Properties of CoO_x and MnO_x: Fundamental Factors Affecting the Catalytic Performance in the Oxidation Process of VOCs. *Catalysts* **2022**, *12*, 1134. [\[CrossRef\]](#)
43. Rajesh, H.; Ozkan, U.S. Complete Oxidation of Ethanol, Acetaldehyde and Ethanol/Methanol Mixtures over Copper Oxide and Copper-Chromium Oxide Catalysts. *Ind. Eng. Chem. Res.* **1993**, *32*, 1622–1630. [\[CrossRef\]](#)
44. Jirátořá, K.; Kovanda, F.; Ludvíková, J.; Balabánová, J.; Klempa, J. Total Oxidation of Ethanol over Layered Double Hydroxide-Related Mixed Oxide Catalysts: Effect of Cation Composition. *Catal. Today* **2016**, *277*, 61–67. [\[CrossRef\]](#)
45. Jirátořá, K.; Mikulová, J.; Klempa, J.; Grygar, T.; Bastl, Z.; Kovanda, F. Modification of Co-Mn-Al Mixed Oxide with Potassium and Its Effect on Deep Oxidation of VOC. *Appl. Catal. Gen.* **2009**, *361*, 106–116. [\[CrossRef\]](#)
46. Morales, M.R.; Barbero, B.P.; Cadús, L.E. Evaluation and Characterization of Mn-Cu Mixed Oxide Catalysts for Ethanol Total Oxidation: Influence of Copper Content. *Fuel* **2008**, *87*, 1177–1186. [\[CrossRef\]](#)
47. Agüero, F.N.; Barbero, B.P.; Gambaro, L.; Cadús, L.E. Catalytic Combustion of Volatile Organic Compounds in Binary Mixtures over MnO_x/Al₂O₃ Catalyst. *Appl. Catal. B Environ.* **2009**, *91*, 108–112. [\[CrossRef\]](#)
48. Li, X.; Zheng, J.; Liu, S.; Zhu, T. A Novel Wormhole-like Mesoporous Hybrid MnCoO_x Catalyst for Improved Ethanol Catalytic Oxidation. *J. Colloid Interface Sci.* **2019**, *555*, 667–675. [\[CrossRef\]](#)

Disclaimer/Publisher's Note: The statements, opinions and data contained in all publications are solely those of the individual author(s) and contributor(s) and not of MDPI and/or the editor(s). MDPI and/or the editor(s) disclaim responsibility for any injury to people or property resulting from any ideas, methods, instructions or products referred to in the content.